Nonlinear Analytical Analysis of External Rotor Permanent-Magnet Synchronous Motor

Zhaokai Li[1], Xiaoyan Huang[1], *Member IEEE*, Zhuo Chen[1], Tingna Shi[1], *Member IEEE*, Yan Yan[1]

[1]College of Electrical Engineering, Zhejiang University, Hangzhou, 310027, China

This paper proposed a nonlinear analytical model (NAM) for external rotor permanent-magnet synchronous motor (ER-PMSM) considering both rotor and stator saturation. The improved magnetic equivalent circuit (IMEC) is introduced to accurately describe the saturation effect of rotor and stator. The air-gap reluctance is replaced by magnetic flux source and therefore the size of IMEC can be reduced while keeping high accuracy. For the air-gap field calculation, the analytical solution will be obtained based on the modified boundary condition from the IMEC. The complex permeance function is extended to represent the slotting effect of ER-PMSM. Hence, the NAM will be numerically solved from the combination of IMEC and analytical air-gap solution. Both finite element analysis (FEA) and experiment demonstrate that the proposed model has high accuracy and requires little time.

***Index Terms*—Nonlinear analytical model, stator and rotor saturation, equivalent magnetic circuit, electromagnetic performance.**

I. Introduction

THE EXTERNAL rotor permanent-magnet synchronous motor (ER-PMSM) has great advantage in high torque density and high efficiency. The analytical analysis for ER-PMSM is similar to that of interior rotor permanent-magnet synchronous motor (IR-PMSM) since most analytical models assume that the iron permeability is infinite [1]-[2]. Nevertheless, ER-PMSM usually has saturated rotor while IR-PMSM has unsaturated rotor. Hence rotor saturation should be paid great attention to for the analytical model of ER-PMSM compared to that of IR-PMSM.

In [1] the analytical air-gap solution combined with complex permeance function (CPM) was introduced to calculate the no-load field of ER-PMSM while in [2] the subdomain technique was used for predicting electromagnetic performance of ER-PMSM. Shen *et al.* investigated the optimal split ratio of ER-PMSM using a simple analytical formula [3]. However, these models neglect the iron saturation. For the analytical models of IR-PMSM, the complex permeance model combined with magnetic circuit was proposed to account for stator saturation [4]. Besides, the subdomain and magnetic circuit hybrid model was introduced to calculate the saturated IR-PMSM with higher accuracy [5]. However, these methods are only suitable for IR-PMSM due to neglecting the rotor saturation.

This paper proposed a nonlinear analytical model to calculate the magnetic field of the whole ER-PMSM considering both rotor and stator saturation. In the proposed model, the improved magnetic equivalent circuit (IMEC) was introduced to simplify the modelling of air-gap region. The magnetic flux source was used to represent influence of air-gap field on the magnetic potential distribution in the rotor and stator according to the IMEC. Then the modified boundary condition will be obtained from IMEC, from which the analytical air-gap field of ER-PMSM is derived. Hence, the magnetic potential solution of IMEC can be numerically obtained. The nonlinear analytical model (NAM) achieves high accuracy and reduces much computation, which is validated by finite element analysis (FEA) and experimental results.

II. Nonlinear Analytical Model

In the proposed NAM, the stator and rotor are represented by the IMEC. The magnetic flux source in the IMEC is obtained from the analytical air-gap field with modified boundary condition. Since the air-gap magnetic reluctance is replaced by the flux source in the IMEC, the numerical solving process of NAM consumes less time. In the air-gap region, the modified boundary condition is determined by the magnetic potential drop of the reluctance on the rotor bore and stator outer surface of the ER-PMSM. Hence, the magnetic field of ER-PMSM is iteratively solved using the NAM.

A. Improved Magnetic Equivalent Circuit for Iron

The IMEC representing the external rotor among the range of one pair pole is shown in Fig. 1. The magnetic flux source φ_{ri} is calculated by the integral of radial air-gap field B_r.

$$\phi_{ri} = R_r l_{ef} \int_{\alpha_{ri}-\theta_{r(i-1)}/2}^{\alpha_{ri}+\theta_{ri}/2} B_r(\alpha, R_r)\, d\alpha \tag{1}$$

where R_r and l_{ef} are the radius of rotor bore and the effective length, respectively. α_{ri} and θ_{ri} represent the center position and the interval between the center position for rotor field integral.

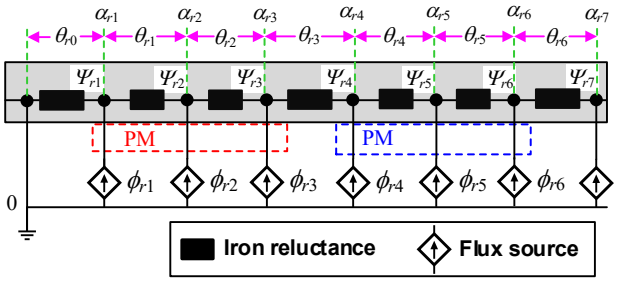

Fig. 1 The schematic view of IMEC for the rotor of ER-PMSM

In Fig. 1, the iron reluctances are distributed according to the displacement of permanent magnet (PM), which means that the magnetic flux is regard as uniform in each magnetic path of the iron reluctance. Hence the rotor magnetic potential Ψ_{ri} is used to obtain the modified boundary condition on the rotor bore.

$$\varphi(R_r,\alpha)=\frac{(\Psi_{r(i+1)}-\Psi_{ri})(\alpha-\alpha_{ri})}{\theta_{ri}}+\Psi_{ri} \qquad (2)$$

where $\alpha_{ri}<\alpha\leq\alpha_{r(i+1)}$ and Ψ_{ri} is the node magnetic potential of rotor. The solution of the rotor IMEC can be numerically calculated based on Kirchhoff's Law.

$$f(\mathbf{\Psi_r})=\mathbf{A_r}\mathbf{\Lambda_r}\mathbf{A_r}^{\mathrm{T}}\mathbf{\Psi_r}-\mathbf{\Phi_r}=0 \qquad (3)$$

where $\mathbf{\Psi_r}$ and $\mathbf{\Phi_r}$ are matrix form of Ψ_{ri} and φ_{ri}, respectively. $\mathbf{\Lambda_r}$ and $\mathbf{A_r}$ are branch permeance matrix and node incidence matrix for rotor IMEC.

In the inner stator, the IMEC is also manipulated to represent the field distribution of stator yoke, stator tooth and the slot, as shown in Fig. 2. Similarly, the magnetic flux source flowing into the stator φ_{sj} is calculated as

$$\phi_{sj}=R_s l_{ef}\int_{\alpha_{sj}-\theta_{s(j-1)}/2}^{\alpha_{sj}+\theta_{sj}/2}B_r(\alpha,R_s)\,d\alpha \qquad (4)$$

where R_s is the radius of stator outer surface. α_{sj} and θ_{sj} represent the center position and the interval between the center position for stator field integral.

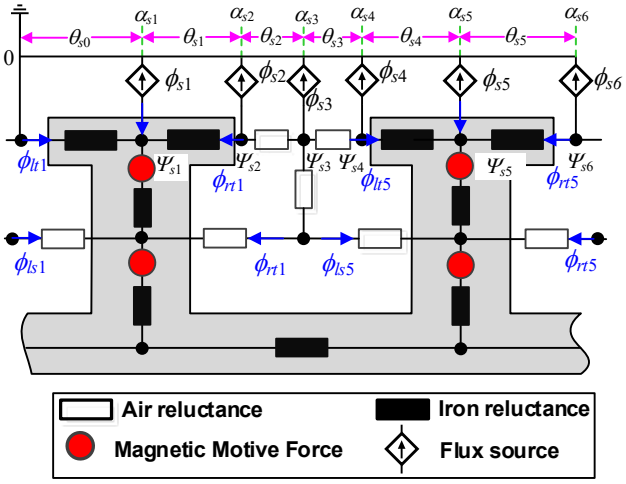

Fig. 2 The schematic view of IMEC for the stator of ER-PMSM.

As the magnetic reluctances along the stator tooth shoe and slot opening are equivalent to the magnetic potential along the stator outer surface, the other modified boundary condition is obtained as

$$\varphi(R_s,\alpha)=\frac{(\Psi_{s(j+1)}-\Psi_{sj})(\alpha-\alpha_{sj})}{\theta_{sj}}+\Psi_{sj} \qquad (5)$$

where $\alpha_{sj}<\alpha\leq\alpha_{s(j+1)}$ and Ψ_{sj} is the node magnetic potential among tooth shoe and slot opening reluctances. According to Kirchhoff's Law, the stator IMEC can be solved using

$$f(\mathbf{\Psi_s})=\mathbf{A_s}\mathbf{\Lambda_s}(\mathbf{A_s}^{\mathrm{T}}\mathbf{\Psi_s}-\mathbf{E_s})-\mathbf{\Phi_s}=0 \qquad (6)$$

where $\mathbf{\Psi_s}$ and $\mathbf{\Phi_s}$ are matrix form of Ψ_{sj} and φ_{sj}, respectively. $\mathbf{\Lambda_s}$ and $\mathbf{A_s}$ are branch permeance matrix and node incidence matrix for stator IMEC.

B. Analytical Air-gap Calculation

As the iron nonlinearity and saturation effect is considered in the IMEC and the modified boundary condition is obtained, the air-gap field can be analytically predicted for ER-PMSM. The total air-gap field can be divided into two parts. One is the PM component obtained by solving the Poisson's equation in the PM region and Laplace's equation in the air-gap region, whose boundary condition is a constant value [6]. The expression of slotless air-gap field for radial and tangential PM component (B_{mr} and $B_{m\alpha}$) can be found in [6]. The other is defined as IMEC-based component, which solves Laplace's equation in the whole air-gap region (neglecting PM) and satisfies the modified boundary condition (2) and (5). Therefore, radial and tangential IMEC-based component of air-gap field is expressed as

$$\begin{aligned}B_{imec\_r}=&\frac{2\mu_0}{\pi}\sum_{i=1}^{6p}\sum_{v}\frac{(\Psi_{r(i+1)}-\Psi_{ri})}{v\theta_{ri}}\frac{1+(R_s/r)^{2v}}{1-(R_s/R_r)^{2v}}\frac{r^{v-1}}{R_r^{\,v}}*\\&\sin(v\theta_{ri}/2)\sin\{v[\alpha-(\alpha_{ri}+\alpha_{r(i+1)})/2]\}+\\&\frac{2\mu_0}{\pi}\sum_{j=1}^{4Q_s}\sum_{v}\frac{(\Psi_{s(j+1)}-\Psi_{sj})}{v\theta_{sj}}\frac{1+(R_r/r)^{2v}}{1-(R_r/R_s)^{2v}}\frac{r^{v-1}}{R_s^{\,v}}*\\&\sin(v\theta_{sj}/2)\sin\{v[\alpha-(\alpha_{sj}+\alpha_{s(j+1)})/2]\}\end{aligned} \qquad (7)$$

$$\begin{aligned}B_{imec\_\alpha}=&\frac{2\mu_0}{\pi}\sum_{i=1}^{6p}\sum_{v}\frac{(\Psi_{r(i+1)}-\Psi_{ri})}{v\theta_{ri}}\frac{1-(R_s/r)^{2v}}{1-(R_s/R_r)^{2v}}\frac{r^{v-1}}{R_r^{\,v}}*\\&\sin(v\theta_{ri}/2)\sin\{v[\alpha-(\alpha_{ri}+\alpha_{r(i+1)})/2]\}+\\&\frac{2\mu_0}{\pi}\sum_{j=1}^{4Q_s}\sum_{v}\frac{(\Psi_{s(j+1)}-\Psi_{sj})}{v\theta_{sj}}\frac{1-(R_r/r)^{2v}}{1-(R_r/R_s)^{2v}}\frac{r^{v-1}}{R_s^{\,v}}*\\&\sin(v\theta_{sj}/2)\cos\{v[\alpha-(\alpha_{sj}+\alpha_{s(j+1)})/2]\}\end{aligned} \qquad (8)$$

The complex permeance function is manipulated for ER-PMSM to account for slotting effect [7]. It builds up the relationship between slotted and slotless air-gap field using four transformations from slotless K domain to slotted S domain

$$T=\ln(K) \qquad (9)$$

$$W=e^{-j\frac{\pi}{g}\left[T-\ln(R_s)-j\frac{\theta_s}{2}\right]} \qquad (10)$$

$$\begin{aligned}Z=-j\frac{g'}{\pi}\Bigg[&\ln\left(\frac{(b-1)W+(b-a)+(b-1)\sqrt{W-a}\sqrt{W-b}}{(b-1)W+(b-a)+(1-b)\sqrt{W-a}\sqrt{W-b}}\right)\\&-2\frac{b-1}{\sqrt{b}}\tan^{-1}\sqrt{\frac{W-b}{b(W-a)}}\Bigg]+\ln R_s+j\theta_1\end{aligned} \qquad (11)$$

$$S=e^{Z} \qquad (12)$$

where θ_1 is half of the tooth shoe angle and θ_s is the angle per slot and tooth. a, b and g' are defined in [7]. Hence the complex permeance function can be calculated as

$$\lambda=\frac{k}{s}\frac{\omega-1}{\sqrt{(\omega-a)(\omega-b)}}=\lambda_a+j\lambda_b \qquad (13)$$

The total radial and tangential air-gap field can be calculated as

$$B_r=(B_{mr}+B_{imec\_r})\lambda_a+(B_{m\alpha}+B_{imec\_\alpha})\lambda_b \qquad (14)$$

$$B_\alpha=(B_{m\alpha}+B_{imec\_\alpha})\lambda_a-(B_{mr}+B_{imec\_r})\lambda_b \qquad (15)$$

C. Calculation of ER-PMSM Performance

As the flux distribution in the IMEC is obtained, the flux linkage of ER-PMSM for each phase ψ_{ABC} is calculated as

$$\psi_{ABC} = N_c \sum_{k=1,5,\cdots}^{\tau} [\varphi_{sk} + \varphi_{ltk} + \varphi_{lsk} + \varphi_{rtk} + \varphi_{rsk}] \quad (16)$$

where φ_{ltk}, φ_{lsk}, φ_{rtk}, and φ_{rsk} are the tooth-tip and slot leakage flux on the left and right side of each tooth (see Fig. 2). Hence the back-EMF is expressed as.

$$E_{ABC} = -\frac{d\psi_{ABC}}{dt} \quad (17)$$

The electromagnetic torque is calculated using Maxwell tensor theory [1].

$$T_e = \frac{1}{\mu_0} l_{ef} r_0^2 \int_0^{2\pi} B_r(\alpha, r_0) B_\alpha(\alpha, r_0) d\alpha \quad (18)$$

where r_0 is the radius of a closed loop path in the air-gap.

III. FE Simulation and Experimental Validation

An ER-PMSM with double-layer concentrated winding is analyzed using Ansys Maxwell and then it is manufactured to validate the proposed model, Fig. 3. The main parameters are given in TABLE I. The small permeability of rotor iron will make the rotor saturation severe so that the difference between the NAM and CPM become significant.

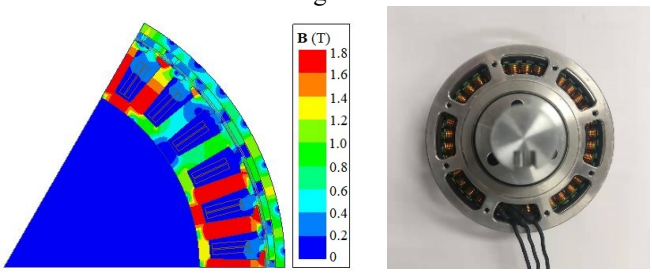

Fig. 3 The 42-pole/36-slot prototype ER-PMSM in the (a) FEA and (b) experiment.

TABLE I
THE MAIN PARAMETERS OF ER-PMSM

	Parameter	Value	Parameter	Value
Stator	Outer diameter	81 mm	Inner diameter	60.5 mm
	Iron material	DW315		
Magnet	Material	NdFe30	Thickness	1 mm
	Remanence	1.1 T	Relative permeability	1.04
Rotor	Outer diameter	87 mm	Inner diameter	84 mm
	Iron material	AISI 420	Effective length	8 mm

Fig. 4 illustrates that the air-gap field prediction at rated load is accurate using NAM but exhibits huge errors using CPM. For the back EMF calculation, NAM achieves excellent accuracy compared with FEA and experiment but CPM still overestimates it, as shown in Fig. 5. Besides, NAM gives a similar waveform of electromagnetic torque compared to that of FEA but the error of CPM can reach to nearly 47%, as shown in Fig. 6.

The nonlinearity of ER-PMSM will greatly affected by load condition. Hence, the average torque and induced voltage predicted using NAM, CPM, and FEA are compared under different input current, as shown in Figs. 7-8. NAM can accurately show motor saturation level under all circumstances. For CPM, as current grows, the voltage error of 1st order harmonic varies in a certain range while the error of 3rd order induced voltage significantly increases. CPM shows low accuracy for predicting total induced voltage.

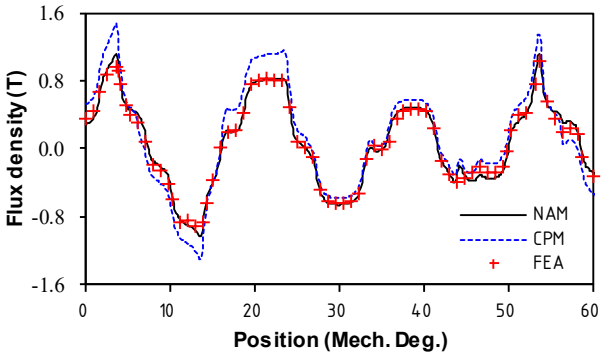

(a)

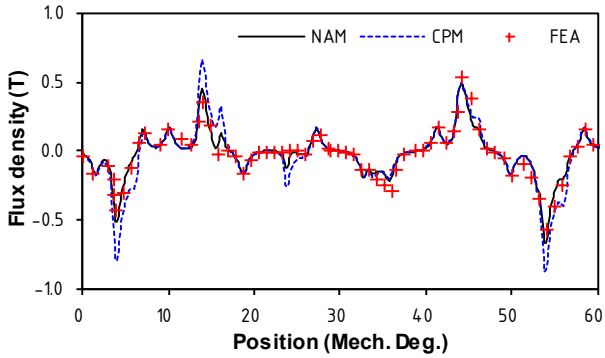

(b)

Fig. 4 The (a) radial and (b) tangential air-gap field distribution along the central air-gap path.

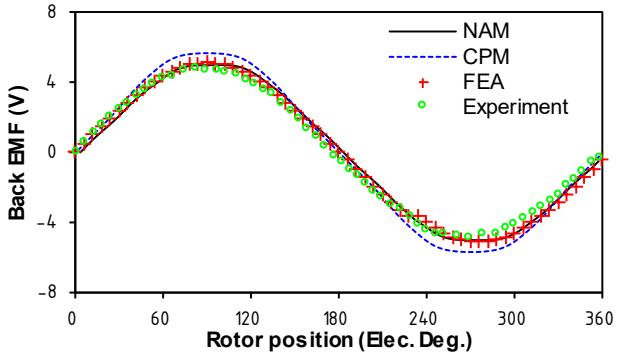

Fig. 5 The measured and calculated back EMF waveform of Phase A at no load condition.

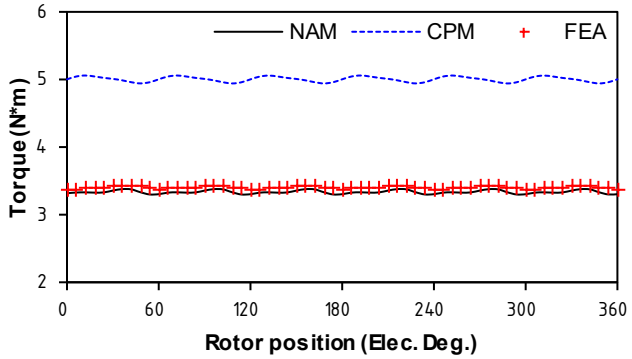

Fig. 6 The comparison of torque waveform for ER-PMSM at rated load (I_A=40A).

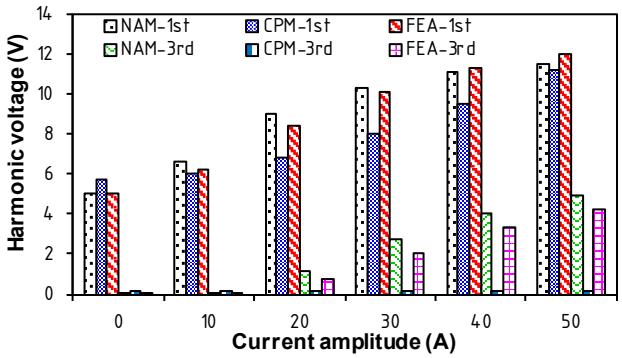

Fig. 7 The comparison of 1st order and 3rd order harmonic induced voltage for ER-PMSM at different load.

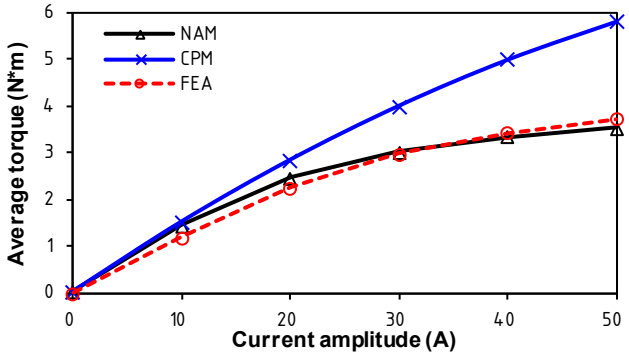

Fig. 8 The comparison of average torque for ER-PMSM at different load.

As the rotor saturation is special to ER-PMSM, the rotor outer diameter is adjusted while other parameters keep unchanged to verify the accuracy of NAM at different saturation level. Figs. 9-10 show the NAM predictions of back EMF and rated torque agree well with FEA results. Besides, as rotor outer diameter increases, the rotor saturation becomes less significant and therefore the CPM predictions which neglect saturation effect get close to NAM calculations.

Even the NAM achieved high accuracy, it only consumed 5.2s and 9.3s to calculate ER-PMSM at no load and rated load condition, respectively. However, it took FEA 119s and 126s to obtain the results under the same condition. CPM only required 0.95s and 1.1s to predict the no load and rated load performance of ER-PMSM, but its accuracy is low and cannot analyze the influence of rotor and stator shape in the design of ER-PMSM due to the assumption of infinite iron permeability.

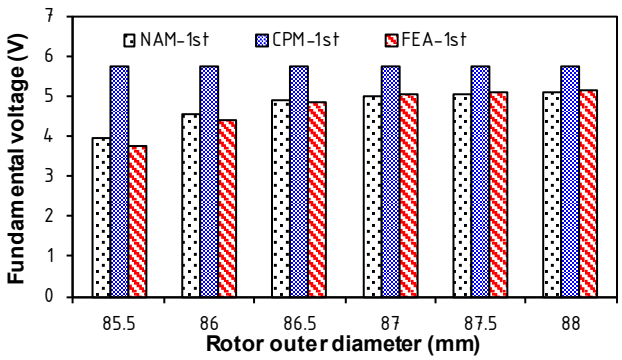

Fig. 9 The influence of rotor outer diameter on the back EMF at no load condition.

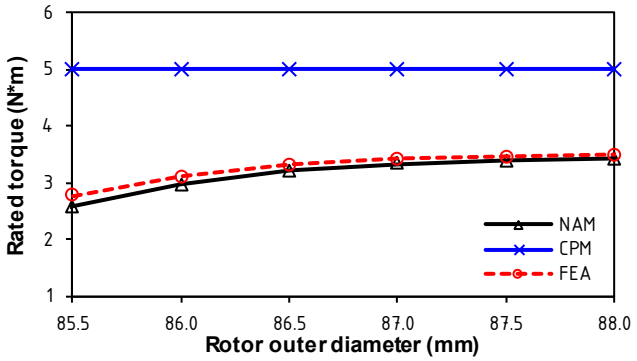

Fig. 10 The influence of rotor outer diameter on the rated torque (I_A=40A).

IV. Conclusion

In this paper, the NAM is proposed for accurate field prediction in the ER-PMSM accounting for both rotor and stator saturation. The air-gap reluctance is replaced by magnetic flux source in the IMEC while the rotor and stator saturation is represented by the IMEC. The IMEC will give the modified boundary condition to obtain the analytical air-gap field solution. The complex permeance function is used to account for slotting effect. Hence, both iron and air-gap field is numerically calculated based on the NAM. The proposed model shows great accuracy and reduces the computational time, which is demonstrated by both FEA and experimental results.

Acknowledgment

This work was supported by the Key R&D Program of Zhejiang (2019C01075), National Natural Science Foundation of China (51922095) and the Ningbo Science and Technology Innovation 2025 Major Project (2018B10001).

References

[1] C. Ma, C. Chen, Q. Li, H. Gao, Q. Kang, J. Fang, H. Cui, K. Teng, and X. Lv, "Analytical calculation of no-load magnetic field of external rotor permanent magnet brushless direct current motor used as in-wheel motor of electric vehicle," *IEEE Trans. Magn.,* vol. 54, no. 4, pp. 1-6, Apr. 2018.

[2] H. Moayed-Jahromi, A. Rahideh, and M. Mardaneh, "2-D analytical model for external rotor brushless PM machines," *IEEE Trans. Energ. Conv.,* vol. 31, no. 3, pp. 1100-1109, Sept. 2016.

[3] Y. Shen and Z. Q. Zhu, "Analytical prediction of optimal split ratio for fractional-slot external rotor PM brushless machines," *IEEE Trans. Magn.,* vol. 47, no. 10, pp. 4187-4190, Oct. 2011.

[4] L. J. Wu, Z. Li, D. Wang, H. Yin, X. Huang and Z. Q. Zhu, "On-load field prediction of surface-mounted PM machines considering nonlinearity based on hybrid field model," *IEEE Trans. Magn.,* vol. 55, no. 3, pp. 1-11, March 2019.

[5] L. J. Wu, Hao Ying, Dong Wang, and Youtong Fang, "On-load field prediction in SPM machines by a subdomain and magnetic circuit hybrid model," *IEEE Trans. Ind. Electron.,* in press.

[6] Z. Q. Zhu, D. Howe, and C. C. Chan, "Improved analytical model for predicting the magnetic field distribution in brushless permanent-magnet machines," *IEEE Trans. Magn.,* vol. 38, no. 1, pp. 229-238, Jan 2002.

[7] D. Zarko, D. Ban, and T. A. Lipo, "Analytical calculation of magnetic field distribution in the slotted air gap of a surface permanent-magnet motor using complex relative air-gap permeance," *IEEE Trans. Magn.,* vol. 42, no. 7, pp. 1828-1837, July 2006.